Hexavalent Chromium Removal Using Ultraviolet Photocatalytic Reactor

by

Heather O'Neal Stancl

A Thesis Presented in Partial Fulfillment
of the Requirements for the Degree
Master of Science

Approved November 2013 by the
Graduate Supervisory Committee:

Paul Westerhoff, Chair
Candace Chan
Kiril Hristovski

ARIZONA STATE UNIVERSITY

December 2013

ABSTRACT

Hexavalant chromium (Cr(VI)) poses an emerging concern in drinking water treatment with stricter regulations on the horizon. Photocatalytic reduction of Cr(VI) was investigated as an engineering scale option to remove hexavalent chromium from drinking or industrial waters via a UV/titanium dioxide (TiO_2) process. Using an integrated UV lamp/ceramic membrane system to recirculate TiO_2, both hexavalent and total chromium levels were reduced through photocatalytic processes without additional chemicals. Cr(VI) removal increased as a function of higher energy input and TiO_2 dosage, achieving above 90% removal for a 1g/L dose of TiO2. Surface analysis of effluent TiO_2 confirmed the presence of chromium species.

DEDICATION

I dedicate this thesis to the people who have loved me through the last year and a half. Though I am far away, my family and family of friends have provided immense support, love, encouragement, and joy. You have continued to remind me that I can do anything I put my mind to, and helped me to persevere. To my new Arizona family, thank you for the lunches, dinners, the advice, the help and support and the late nights with tough issues. Living life together has brought me to a place of success and overcoming amidst the desert.

ACKNOWLEDGMENTS

I wish to thank all of my committee members who graciously served to advise, troubleshoot, review and provide their expertise and equipment (Dr. Kiril Hristovski, Dr. Candace Chan). An extra thank you goes to Dr. Paul Westerhoff, who has trained me in chemistry, engineering and plumbing over the last year and a half. You have provided countless insights for how to proceed in research. I am also deeply grateful for the fellow researchers who have contributed to this work: Kyle Doudrick, Xiangyu Bi, Alexandra Bowen, Michelle Barry, David Hanigan, Marisa Masles and Ting Yang, as well as Omer Karovic for his engineering expertise and support throughout the process.

I would also like to thank and acknowledge the National Science Foundation (CBET 1132779), the United States Environmental Protection Agency (RD835175), Arizona's Salt River Project, and the Ira A. Fulton Schools of Engineering Dean's Fellowship and Arizona State University for funding my work.

TABLE OF CONTENTS

Page

LIST OF FIGURES

CHAPTER 1

INTRODUCTION

Experimental Background

Chromium is a drinking water contaminant with natural and industrial sources that poses potential human health risks. A 2010 study by the U.S. Environmental Working Group mapped chromium concentration data found for tap waters across the nation, revealing upwards of 1ppb and even 10ppb Cr(VI) concentrations found in drinkable waters (Sutton, 2010). A significant complication arises in water distribution systems, where water endures long contact times with disinfection residuals and reduced and released trivalent chromium, Cr(III), can re-oxidize to form Cr(VI); this necessitates complete removal of all chromium species (Lai and McNeill 2006). Both hexavalent chromium (Cr(VI)) and trivalent chromium (Cr(III)) have been linked to negative health effects, including, but not limited to: increasing risk for cancers (respiratory, prostate, lymphoma, leukemia, bone, and stomach), gastro-intestinal system disruption, uptake, accumulation and toxicity in vital organs, damage to DNA and gene mutation (Costa 1997; Dayan and Paine 2001; Sedman, et al. 2006; Beaumont, et al. 2008). Though current regulation is set at 100ppb for total chromium (Barrera-Diaz, et. al 2012), with enforceable maximums for hexavalent chromium expected to lower significantly within the coming years (California EPA 2011), increasing options for complete removal of total chromium species in addition to hexavalent chromium is becoming critical.

Treatment options for Cr(VI) have traditionally fallen into five treatment classifications (Sharma et. al 2008): coagulation-precipitation-filtration, adsorption to different media, ion exchange, membrane technology and electrodialysis, and biological

removal. Major concerns with these methods arise in the scalability to treat and meet large scale demand, ranging from cost and availability of materials to operational costs, pH requirements, and reliability (McNeill, et al. 2012; Owlad, et. al 2009). Although Cr(VI) absorbs poorly to most metal oxides, an emerging sixth category are various catalytic reduction techniques that reduce Cr(VI) and sorb Cr(III), which is readily accepted by metal oxides at neutral pH. Here we propose a combined photocatalytic reduction followed by sorption of the by-product to the photocatalyst. A number of studies have demonstrated success using uniquely synthesized and modified semiconductor photocatalysts for UV and visible light removal of hexavalent chromium. (Vignesh, et. al 2013; Chakrabarti, et. al 2009; Li, et. al 2012). Though they prove efficacy of using catalysts for Cr(VI) reduction and removal, many studies encountered pH limitations and would incur immense cost and energy demand for added chemicals and catalyst preparation upon scale-up. A stable, proven, and preferable photocatalyst may be titanium dioxide (TiO_2), known for its unique surface properties, commercial pricing and availability, and treatment capacity for chromium as well as successful photocatalytic reduction of nitrate and other oxo-anions (Doudrick, et al. 2012).

Previous studies with TiO_2 and Cr(VI) removal indicate potential interferences and interactions with dissolved organics (Wang, et al. 2008) and other ions, but far higher success in removal than other toxic metal ions (Chen and Ray 2001). This is attributable to the mutual oxidation and reduction potential of TiO_2 under UV light. While UV/TiO_2 is usually viewed as an advanced oxidation process (AOP) because it produces hydroxyl radicals to oxidize pollutants, it is well known that reduction (i.e. hole scavenging) also occurs on TiO_2 surfaces.

Studies on hexavalent chromium and TiO_2 under UV irradiation have the highest rates observed at pH 4, with 10x lower rate at neutral pH (Ku and Jung, 2001). Increasing the Cr/Ti ratio led to diminished reaction rate ~2x in an oxygen rich system and ~8x in anoxic conditions (Yang, et. al, 2012). At pH greater than 4, a concern is the resultant fouling of TiO_2 by chromium hydroxides (Gimenez, et. al, 1996). Therefore, in more neutral natural waters, TiO_2 fouling could greatly diminish the reduction capacity for hexavalent chromium. Though such studies have compiled a fundamental knowledge base of hexavalent chromium removal over TiO_2 photocatalysts, thus far, there have been no published studies on the engineering implications of Cr(VI) photocatalytic reduction.

The goal of this paper is to demonstrate the viability of photocatalytic reduction of Cr(VI) and removal of residual Cr(III) byproducts from drinking water using an integrated reactor system with UV lamps to irradiate water containing varied dosage TiO_2 slurries with recovery of TiO_2 across a ceramic membrane. This was completed to (1) demonstrate the successful removal of aqueous hexavalent and trivalent chromium through varying water matrix, catalyst dosage, and energy input, (2) determine efficacy of a 'chemical-free' method using only commercial TiO_2 and UV irradiation for removal, (3) distinguish between different sorbed Cr-species on the TiO_2 after photocatalytic reduction of Cr(VI).

Photon Generation in Hg and Xe Low and Medium Pressure Lamps

Photocatalytic processes employ mercury and ‘mercury-free’ xenon lamps to provide light irradiation to activate the catalyst. Depending on the chemical constituent of interest, either low pressure or medium pressure lamps are utilized, the former with sharper peaks and singular wavelength ultraviolet (UV) outputs and the latter with a

broader spectrum of available wavelength in the UV and low wavelength visible range. The lamp properties that induce these output differences relate to the material utilized (Hg/Xe), the abundance of that material, as well as pressure of the system.

Lamp Mechanics

Lamps consist of four crucial elements to functionality: gaseous metal ions, electron current induced by a potential difference across an electrode, a noble and inert gas, and a light permeable/impermeable sleeve depending on the desired photonic output. Thus, from the AC current output from the wall, an electric current is induced across a +/- electrode pair within the lamp housing. This induces a flow of electrons throughout this sleeve. Gaseous metal ions, most commonly mercury, exist in a mobile state within the sleeve, coexisting with the inert gas. The inert gas, most commonly argon, is added to serve as the means for pressure modification and additionally to reduce electron collisions with the sleeve wall.

Thus, upon lamp turn-on, a flow of electrons driven by the potential difference between the two electrodes propagates through the argon-mercury media and undergoes collisions. Electron-wall collisions induce a release thermal heat upon electron energy exchange, creating no meaningful photonic output. Electron-argon collisions do not significantly degrade the energy of the electrons, while leaving the argon unchanged and thus represent a quasi-neutral energy transaction. The important collisions for photon emission are the electron-mercury ion collisions, in which mobile electrons transfer energy to mobile mercury electrons. This energy transfer leads to a promotion of an electron within the mercury valence to an excited state. Upon relaxation of this electron

to the pre-existing state, or another quantized level of lesser energy, a photon is emitted. Based on the resonance energy of the electron excitation and return, the photon will emit at a particular wavelength. Higher energy discharge corresponds to a shorter wavelength emission.

The inert gas is essential to the process of buffering the electrons from the tube walls to prevent heat transfer upon collision. Additionally, this gas increases the frequency of elastic collisions between gaseous constituents, thereby reducing the mean free path of electrons (and their energy upon collision). This property can be manipulated to increase the number of spectral output wavelengths or to increase high quality low wavelength output by pressure modification. Additionally, energy loss in collisions with the inert gas does not diminish the electron energy level to the extent that the excitation of metal atoms is negated by additional collisions (Flesch 2006).

Mercury Lamps

Low pressure mercury lamps are pervasive as efficient fluorescent lamps (Wani 1994), but are also widely implemented in photocatalytic and germicidal processes due to their wavelength of emission. The emission spectrum of mercury has two high efficiency resonance lines of wavelength 253.7nm and 184.9nm at low pressure (Voronov 2008). The exclusive emission of these two wavelengths is related to the mean free path the electron is able to travel within the lamp. Within a low pressure system, the mean free path of electrons is sufficiently large that it can gain enough velocity, and thereby kinetic energy ($KE=1/2mv^2$), that collision with mercury ions produces significant electron excitation – velocities too high result in electron annihilation. The baseline velocity of

the electrons may be altered by changing the potential difference between the electrodes. As discussed, the introduction of the inert gas helps to mitigate energy lost in electron-wall collisions and maintain a desired balance of electron velocity and collision frequency. If the pressure is too low, then the probability of electron-mercury collisions diminishes and the likelihood of annihilation increases. At a reasonably low pressure, however, sufficiently high energy collisions may occur resultant in the desired 6^3P_1 to 6^1S_0 transition between resonance states in the mercury that provide a photonic output at 253.7nm (Loo et al. 2004).

At pressures between 1-10 bar, what constitutes the medium pressure range, the mean free path length of electrons is shortened due to heightened collision frequency resultant from higher mercury vapor pressure. Thus, an increased applied voltage is necessary to induce electron-ion collisions of sufficient energy to produce photons. The wavelength outputs of medium pressure lamps are longer than those of low pressure lamps due to the diminished energy transfer from electrons to the mercury valence. Due to the higher non-radiative losses and wall losses, the ultraviolet efficiency of medium pressure lamps is lower than that of low pressure lamps (Giller 2000).

Xenon Lamps

Due to emerging environmental and health concerns from mercury residual from lamp disposal and failure in addition to point of use concerns with warm up time, xenon lamps are being pursued as alternatives (Schaefer et al. 2007). Xenon is currently the most promising mercury replacement due to strong resonance and excimer emissions in the VUV region, from 100-200nm (Jinno, et al. 2007). Xenon lamps similarly utilize a

quartz envelope and electric potential between to electrodes; however, they only employ xenon – a noble gas – to provide excitation from electron collisions against a neon gas background. Pulsed xenon-neon lamp emissions have two peaks, one during the discharge current and a second during the afterglow period. Depending on the partial pressure of xenon in the envelope, the afterglow intensity varies – it increases with increasing Xe content (Jinno, Korukawa and Aono 1999). Discharge wavelengths of pulsed xenon-neon lamps are 147nm and 172nm. Additional output wavelengths between 200-300nm have been reported (Liang, et al. 2003). Xenon efficiencies and luminosities are generally lower than mercury lamps, although for the 147nm output 75% efficiencies have been obtained (Uhrlandt et al. 2005).

Bandgap Influence on Photon Absorption

Absorption of photons with greater energy than the bandgap of a photocatalyst generates conduction band electrons and subsequently, valence band holes. This 'bandgap energy' is the threshold of energy needed for the semiconductor to undergo redox upon absorption of a photon. Influent photons must meet this minimum threshold of energy in order to activate the photocatalyst, whereas other photonic wavelengths may be absorbed but with insufficient energy to promote electron-hole separation. An example of successful activation for a titanium dioxide catalyst is as follows:

$$TiO_2 + h\nu \rightarrow TiO_2(e^-_{cb} + h^+_{vb})$$

where e^-_{cb} represents the electron promoted to the conduction band and h^+_{vb} represents the hole that theoretically remains in the valence band. Holes may also be mobile depending on the influent energy, structure of the lattice, and defect occurrence.

In an ideal semiconductor, there are no energy states within the band gap. A 'fundamental absorption' occurs if the light absorption is due only to the transfer of e^- from the valence band to the conduction band (Seeger 2002) and not resultant in lattice vibrations. Because electrons can only have discrete energy values, transitions between energy levels can either be spontaneous or instigated by photons (Schiavello 1997). For TiO_2, the band gap is well studied, and consensus values are 3.03 eV for rutile and 3.20 eV for anatase (Scanlon et al. 2013). Thus, for a titanium dioxide nanoparticle, a maximum photonic wavelength (minimum energy) is required for excitation:

$$E = \frac{hc}{\lambda}$$

$$3.2eV = 5.12x10^{-19}J = \frac{6.62606957 \times 10^{-34} \frac{\mathrm{m}^2\ \mathrm{kg}}{s} x\ 2.998x10^{8} \frac{m}{s}}{\lambda}$$

$$\lambda = 3.88x10^{-7}m = 388nm$$

where h (Planck's constant) = $6.62606957 \times 10^{-34}$ m^2 kg / s, 1 eV = 1.6×10^{-19} joules, c (speed of light) = $2.998x10^8$ m/s, and a joule is equal to 1 kgm^2/s^2. From this relationship of bandgap, or the energy that must be overcome to excite an electron into the conduction band of TiO_2, and wavelength, it is shown that a maximum wavelength of 388nm can activate TiO_2 electrons. Due to the inverse relationship of energy and wavelength, lower wavelength light must be utilized to have sufficient energy to excite TiO_2 electrons photocatalytically.

However, impurities within the crystal lattice may introduce allowable levels for electrons that are within the band gap. Influent photons below the bandgap threshold energy cause perturbations within the vibrational modes of the crystal lattice or

absorption within impurities in the lattice (Elliott and Gibson 1974). This is also impacted electronically in the Fermi energy. The Fermi energy, E_F, is the energy of the highest occupied electronic state at zero kelvin. At 0K, the hypothetical Fermi energy represents the boundary of filled and unfilled electron energy states, where all states below E_F are full, and all electronic states above E_F are empty. Upon excitation, electrons move to higher energy states thus creating a new and ephemeral excited electron configuration. In the bulk of a perfect semiconductor, no electrons exist at the Fermi energy level because there are no electronic states available, i.e. the density of states is zero at the Fermi level. However, in a non-ideal semiconductor, structural defects allow for states to exist in the bandgap above zero kelvin.

Resultant excitation depends on energy of the light, inclusive of frequency, wavenumber or wavelength of the photon. If the final and initial energy state do not fulfill the resonance condition, photon absorption will not occur. The absorption properties depend not only on the chemical identity of the substance and light wavelength, but also on the light's angle of incidence and polarization. Semiconductors require visible (for narrow bandgap) or ultraviolet irradiation in order to absorb photons due to the band gap energy requirement. Infrared light cannot be absorbed because the energy is below the bandgap energy. Whenever the photon energy is sufficient to excite electrons from filled valence states to the vacant conduction states, electronic excitation occurs as a result of the light absorption. The minimum energy for these transitions to produce free electrons is a quality intrinsic to materials and varies; the bandgap energy of TiO_2 is 3.2eV. Bound electron-hole pairs, called excitons, exist below the threshold of the conduction band and also participate in recombination reactions.

The existence of a bandgap in a semiconductor has a number of important implications. Outright electrical conductivity is low due to the energy barrier of the bandgap to drive electrons in the conduction band. Additionally, electron-hole pair formation is limited by the input energy required to overcome the gap between the valence and conduction bands. These properties of semiconductors necessitate an added energy, perhaps significant, in order to be meaningfully employed for contaminant reduction.

Mechanistic Assessment of Aqueous Electron/Hole Lifetimes

Ideally, the electrons and holes generated may be utilized to induce chemical reactions at the surface of the metal oxide semiconductor. Fundamental to semiconductor function is the behavior of the p-n junction, where a contact potential exists between the p-type and n-type portions of a semiconductor lattice at equilibrium; this potential contributes to separation of electrons and holes at the n-type and p-type sides, respectively (Moll 1964, 110). If this potential is decreased by increasing the positivity of the p-side, charge carriers may more readily diffuse from regions of majority to minority along a charge gradient. However, if the p-type becomes more negative than the n-type side, the barrier is increased and diffusion is greatly diminished. Thus, to understand and catalyze reactions, the process of production and transport of e^-/h^+ pairs in semiconductors as well as the potential for recombination must first be assessed and accounted for.

Production

Conduction electrons and holes are produced in pairs within a semiconductor and at the surface upon proper irradiation. The rate of production (number per unit volume per unit time) depends on the semiconductor material (energy and momentum needed to produce a pair) in addition to the thermal activity of the surroundings (Adler, Smith and Longini 1964). Temperature changes in the solution may produce sufficient thermal vibrations within the lattice to produce an electron-hole pair via the breaking of a valence bond. More commonly in photocatalytic endeavors, this production is prompted by a light source (photon emission/absorption) that provides sufficient energy to the semiconductor to break a covalent lattice bond.

Transport

Transit time for holes and electrons to reach photocatalyst surface are related to the radius of the particle, R, and a diffusion coefficient of the excited charge carriers $\tau = R^2/\pi D$ (Gratzel and Frank 1982). Thus, for particles between 10-20nm, a common TiO2 nanoparticle size range, transit time from the point of origin within the structure to the surface is in the range of picoseconds. Additionally, the morphology of the space-charge region, the near surface region of charge density that differs from the bulk solution, strongly influences charge carrier transport. Distinct band bending patterns result from either an ohmic contact or Schottky barrier which represent electrical properties of semiconductor-metal interfaces (Kolansinski 2009, 42-45). The Schottky barrier may be defined as a carrier depletion region at the surface that is resultant from the electrical dipole layer rejection of majority charge carriers from the surface toward the bulk

(Seeger 2002, 143). Additionally, variation in surface states (from a nonhomogeneous semiconductor surfaces) provide a potential for disparity between the electron density at the surface relative to the bulk. This difference allows for diffusive transport of electrons to lower density regions.

The valence band wavefunction of TiO_2 particles has a larger curvature than that of the conduction band, indicating that the 'effective' mass of the hole is smaller than that of the electron; therefore, at the surface, there would likely be more photogenerated holes, whereas electrons would be more readily trapped in the interior (Rajh, Poluektov and Thurnauer 2003). Photoactivation may occur via the surface localization of photogenerated charge carriers traveling from the bulk of the semiconducting material (Cunningham 1988). These charge carriers persist longer at the interface (Cunningham, Goold and Fierro 1982).

Recombination, Trapping, and Surface Reactions

Upon band gap irradiation, three primary photochemical processes occur in a colloidal TiO_2 nanoparticle system: 1) recombination, 2) trapping, and 3) reactions with surface adsorbed constituents. Recombination occurs as a thermodynamic mechanism of restoring thermal equilibrium, and it constitutes the largest energy inefficiency of TiO_2. Charge carriers (e^-/h^+) are formed due to the absorption of light into the titanium dioxide nanostructure. Recombination can occur as radiative or non-radiative according to the following equation: $e^-_{cb\ OR\ tr} + h^+_{vb\ OR\ tr} \rightarrow TiO_2 + energy$, where *cb* represents the conduction band, *vb* represents the valence band and *tr* represents a trapped charge carrier (either electron or hole as indicated) (Bahnemann, Dillert and Robertson 2003). With

insufficient transportation rates and/or pathways and external reaction source, i.e., hole scavenger, electron-pair holes will recombine, releasing heat.

Trapping of electrons and holes occurs within the metal oxide lattice and on the surface, slowing recombination rates. There is consensus that electrons prefer trapping at the surfaces of the TiO2, though there is some evidence and theoretical modeling efforts that suggest bulk trapping supersedes surface trapping (Henderson 2011). Upon low temperature irradiation, a small number of electrons are trapped in the interior to produce Ti^{3+} interstitial ions. Electron paramagnetic resonance indicates two types of electron traps in TiO_2 nanoparticles: 1) internal traps with a narrow and axially symmetric EPR signal, and 2) surface traps with broad EPR lines (Rajh, Poluektov and Thurnauer 2003). Hole trapping, however, occurs on oxygen species within and on the titanium dioxide lattice: $Ti^{4+}O^{-}{\blacksquare}Ti^{4+}OH^{-}$ or $Ti^{4+}O^{2-}Ti^{4+}O^{-}{\blacksquare}$ (Howe and Gratzel 1985) dependent on surface modifications to the TiO_2 and temperature treatment.

Recombination may be successfully deferred in through consumption of electrons and holes at the surface of the semiconductor. Reactive electrons available for interface transfer from TiO_2 colloids to surface constituents occur at the surface Ti atoms that are coordinated with solvent molecules (Kolle, Moser and Gratzel 1985). Reactive holes transfer at surface oxygen molecules that are covalently linked to titanium atoms (Micic and Zhang 1993). Radical species generation are postulated as a significant acceptor of surface holes and electrons throughout interfacial transfer, in this case at the solid-liquid interface. This provides both direct and indirect oxidation-reduction pathways. In photocatalytic redox reactions over TiO_2, surface trapped photogenerated holes are the essential to the process, most commonly oxidizing aqueous organic species. In order to

maintain neutrality, a balance of oxidation-reduction reactions must exist as photogenerated electrons (-) and holes (+) are consumed. In order to have successful oxidation-reduction reactions of constituents at the surface of the photocatalyst the following two properties must exist: 1) for reduction, the conduction band have a more negative potential than the reducing species; 2) for oxidation, the valence band must have a more positive potential than that of the oxidizing species. Therefore, the bandgap and contaminant must be band-paired to undergo successful redox reaction.

Metal Oxide Surface Charge and Zeta Potential

Chemistry at the water-metal interface, i.e., of semiconductors, is determined by the reactivity of water on the metal, chemical reactivity changes due to the electrochemical potential and steric and electrostatic effects of the solvent (Taylor and Neurock, 2005). Surface layers can be classified in four categories based the carrier densities of the n-type semiconducting surface (in comparison to the bulk): 1) accumulation layers ($n_s > n_b$), 2) flat band ($n_s = n_b$), 3) depletion layers ($n_s < n_b$ and $p_s \leq n_b$), 4) inversion layers ($p_s > n_b$) with n and p representing the carrier densities at the surface (Berz 1975). The accumulation layer is charge dense, while the depletion layer has a lower charge density than the bulk.

The water layer structure is influenced by the metal, but also by the presence of co-adsorbates, dissociation capacity, and the presence of an electric field created by the ionic species (which would induce a dipole alignment). Subsequently, under varied pH conditions, water molecule alignment changes due to changing surface charge of the metal surface (Kolansinski 2009, 260). The point of zero charge (pH_{pzc}), also called the

isoelectric point, is defined as the pH at which the overall surface charge is neutral. As the pH or potential changes, the net surface charge will change, most often moving more negative with increasing pH and vice versa. For colloidal species, this pH_{pzc} is the point of zero zeta potential. Zeta potential is defined as the potential differential between a surface and the surrounding bulk liquid. The pH_{pzc} is significant because changes in the surface charge (dipole) cause changes in both the adjoining aqueous layer, but also the accessibility for adsorption of other species in solution (cations to negative surfaces and anions to positive surfaces). The zeta potential represents a net surface charge, and thus represents an aggregate sum of charges on the surface – even at very high pH or electric potential a mix of charges will exist on the surface, allowing for diversity of reactivity and surface adsorption capacity though most often the majority of charge is either positive or negative.

Surface charge of metal oxides is additionally highly dependent on pH due to the variation of (de)protonation of surface sites with increasing or decreasing pH. At high pH, the surface sites would be highly deprotonated, and thus surfaces would likely be more negative. A hydroxylated surface can serve as a proton donor (Bronsted acid) or a proton acceptor (Bronsted base). Electrochemical measurements determine the isoelectric point of the surface – the pH value of a solution in contact with the surface that yields an equal concentration of XOH2+ and XO- sites. At this point, the surface has a net charge of zero. A high isoelectric point indicates a strong surface basicity, whereas a low isoelectric point indicates a strong surface acidity. These relationships pertain to the ability to donate or accept electrons and influence adsorbate-substrate charge transfers but do not directly address adsorption energy. Adsorption energy pertains mainly to the

electrostatic and covalent energy. TiO2 for example, would be protonated at low pH, with surfaces covered by –OH groups:

$$\equiv TiOH_2^+ \leftrightarrow \equiv TiOH + H^+ \quad logk_{a1} = -2.5$$

$$\equiv TiOH \leftrightarrow \equiv TiO^- + H^+ \quad logk_{a1} = -8.0$$

which show deprotonation on the surface with increasing pH (Duro, Bruno and Honeyman 2001). In acidic environment, the surface would reflect the first equation with a mix of $TiOH_2^+$ (a very protonated species) and TiOH with excess hydrogen in solution, whereas in an alkaline environment, the surface would reflect the equilibrium of the second equation. Additionally, though the species are the majority in solution, there will be a mix of charges both at low pH and high pH but these equations represent the majority case of the surface charge: (+) at low pH due to the extra hydrogen on the surface and (-) at high pH due to deprotonation with increasing pH.

Electrostatic Surface Complexation Models: Accounting for Ion-Metal Oxide Interactions

Overview of Metal Oxide Surfaces

Metal oxide surfaces experience a surface energy due to an imbalance of forces between atoms, ions and molecules at the surface. Thereby, a finely dispersed solid metal oxide will attempt to reduce its surface area by complexing with adjacent phase molecules and ions, thus decreasing its overall surface energy. In an aqueous matrix, these molecules may coordinate water molecules by dissociative chemisorption, most often leaving hydroxyl groups at the surface. Because of the metal Ti ions in TiO_2 act as Lewis acids (electron pair acceptor), these surface hydroxyl groups may be replaced by

adsorbing oxyanions (Schindler 1981). The charging of a solid surface in a liquid occurs as a result of three mechanisms: 1) ionization or dissociation of surface groups; 2) adsorption or binding of ions from solution onto a charge neutral surface (ion exchangeable surface); 3) charge exchange where charges (protons or electrons) shift to another surface and induce an electrostatic attraction in an acid-base and opposite charge manner (Israelachvili 2011).

Solid-Liquid Interface

The solid-liquid interface can be divided into four regions: the bulk liquid, the bulk solid, the surface of the solid along with its adsorbates, and a region just above the adsorbed layer that is different from the bulk liquid. In aqueous solution, water will complex on the semiconductor surface based on the pH. As such, pH is the master variable that determines the extent of adsorption of aqueous species onto the surface. Basic oxides exhibit a weak covalent energy with respect to the surface OH^{-}bond, but as oxide acidity increases, the covalent energy increases. This is attributable to increasing electronegativity and decreasing ionic radius. Electrostatic energy is more complex due to Coulombic interactions and adsorbate-substrate charge transfers. The overall adsorbate-substrate interaction is influenced by attractive and repulsive interaction with all substrate ions; the charge transfer at this interface is responsible for a charge decrease of both species as hydroxyl groups and surface oxygen lose electrons and protons and surface cations capture electrons (Noguera 1996).

Ion Adsorption

Adsorption of anion species onto metal oxide surfaces occurs through ligand exchange, a common type of specific adsorption, and correlates to the pH of solution (Hingston 1981). An anion and its conjugate acid will experience an increase in adsorption as the pH increases until dissociation is complete (Bowden, et al. 1973), i.e.:

$$HCrO_4^- \leftrightarrow CrO_4^{2-} + H^+ \ pK_a = 5.9 \text{ (Brito et al. 1997)}$$

$$HCr_2O_7^- \leftrightarrow Cr_2O_7^{2-} + H^+ \ pK_a = 1.8 \text{ (Brito et al. 1997)}$$

Thereafter, a decrease in adsorption will occur past the pk_a of the anion/conjugate acid pair. For chromium, it would be expected that above pH 5.9, the majority of the species would be deprotonated and thus experience diminished but existent adsorption rates to the TiO_2 surface.

At the pH_{pzc} of TiO_2 is at pH=6.2, cationic species would more readily adsorb than anionic species due to the reversal in net surface charge. Minimal cation sorption occurs at or below the pH_{pzc}, but above the pH_{pzc}, cations are adsorbed to counterbalance the overall negative surface charge. Part of the net surface charge is also counterbalanced by the exclusion of anion adsorption at higher pH. Therefore, for metal oxides, cation adsorption increases with increasing pH. Cation selectivity is also influenced by changes in oxidation state, which would be represented in this case as Cr(VI) to Cr(III) and their aqueous complexes. With multivalent cations, small changes in pH can lead to relatively large changes in sorption capacity (Kinniburgh and Jackson 1981).

Surface Complexation Models

Whether ions are specifically or nonspecifically adsorbed within the innermost layer (closest to the metal oxide) depends on the electric field strength and the chemical properties of the ions, while the outer Helmholtz layer includes fully solvated ions. The combination of both of these layers forms the electric double layer. The overall surface charge is determined by the compensation of the excess charge of the first layer at the surface (Kolansinski 2009). With preliminary definitions for the electric double layer and a conceptual framework of charge at the surface, surface complexation models will be explored. The diffusive layer model (two layer model), the constant capacitance model, and the triple layer model are utilized to describe chemical reactions at the surfaces of metal oxides.

The constant capacitance model addresses scenarios when surface potentials are small or high ionic strength in the bulk solution compresses the solution side of the electric double layer. In such a case, the surface potential is proportional to the surface charge:

$$\Psi = \frac{\sigma}{C}$$

where Ψ is the potential in volts, σ is the surface charge in Coulombs/m^2, and C is the integral capacitance in Farad/m^2 (Stumm 1992). Assumptions of the constant capacitance model include: 1) all surface complexes are inner-surface complexes; 2) constant ionic medium reference state determines the activity of aqueous species meaning that no surface complexes are formed with background ions; 3) the surface is represented by one plane of charge (Goldberg 1995). This model most closely resembles the Helmholtz double layer because adsorbing ions are directly adjacent to the surface. The diffuse layer

model, also called the two-layer model, makes another set of assumptions: 1) surface complexes are inner-sphere complexes; 2) complexes do not form with the background ions; 3) the surface is represented by two planes of charge. The triple layer model was created with the assumptions that: 1) H+ and OH- ions form the inner-sphere complexes; 2) outer sphere and inner sphere surface complexes are formed by ion adsorption reactions; 3) outer sphere surface complexes are formed by background ions; 4) three planes of charge represent the surface. The surface-solution interface may also be displayed graphically (potential versus distance from particle surface), with the constant capacitance model as sloped line, the two layer model a horizontal and subsequently curved line (the diffuse layer is the boundary), and the triple layer model a sloped line followed by a line of steeper slope and finally a curve representing the three layers and their potential v. distance relationship.

Surface complexation models describe the interaction of anions and metal oxide surfaces as undergoing a chemisorption substitution process where the anion substitutes for water hydrated or hydroxylated surface species (Blesa, et al. 2000). In the constant capacitance or diffusive layer model this would occur in the first coordination sphere, whereas in the triple layer model in the outer layer. It has been shown that the electronic state of the metal in addition to the surrounding solution greatly influence reactivity at the interface, but dynamics within the double layer have not been well documented in literature (Taylor and Neurock 2005).

Photocatalytic Implications

Predicting the viability of photocatalytic processes can, at least preliminarily, be assessed utilizing knowledge of the physics and chemistry of: lamps, semiconductors,

and chemical contaminants of concern. The proper pairing of output wavelength and semiconductor bandgap is essential to photocatalytic functionality, for if excitation does not occur, the only component of change would likely be adsorption due based on the pH, ionic strength, and surface chemistry of the semiconductor. However, if the bandgap energy can be met by irradiation, both electrons and holes become available for reaction with adsorbed contaminants. The proximity of contaminants relates to the zeta potential of the surface, either creating a repulsive or attractive force for the chemical of concern. Additionally, with changing pH, the surface charge changes, inducing different preferences for surface speciation. Without sufficient surface reactivity and electron-hole pair evolution, recombination will dominate, resulting in loss of transformation productivity on the semiconductor surface. However, if electrons (and holes) can be trapped at surface sites, the potential for reaction increases and oxidation-reduction reactions will occur. Thus, the solid-liquid interface plays a significant role in the success of photocatalytic processes. These theoretical predictions can be verified through experimental results to better understand the mechanisms, pathways, and activities of contaminants with semiconductors in an aqueous environment.

CHAPTER 2

MATERIALS AND METHODS

Experimental Methods

Photocatalytic experiments were performed using an integrated UV/ceramic membrane reactor (Photo-Cat® Serial 0700 system, Purifics ES Inc., Ontario, Canada) with a TiO_2 slurry (Figure 1). Purifics' Photo-Cat-L system has been shown to decompose organic compounds (Westerhoff, et al. 2009), disinfect pathagens (Gerrity, et al. 2008), and transform contaminants to less harmful products and remove them from water (Benotti, et al. 2009). The system employs an automated control system to command the reactor, four 220W low pressure UV lamps (253.7nm output), and a ceramic ultrafilter to efficiently target species for removal while producing catalyst free effluent (Figure 1). Employing low pressure lamps of wavelength 253.7 nm, the device is able to target the bandgap of titanium dioxide (3.2 eV; Doudrick, et. al 2012). TiO_2 recirculates throughout the reactor across the lamps during the experiment and is separated from the water at the effluent port through a ceramic ultrafiltration membrane. Experiments were conducted in batch mode, which recirculates water throughout the reactor at a recirculation rate of 20Lpm. A flow through mode was utilized at a flow rate of 2.1Lpm for 625L of both 100ppb and 10ppb Cr(VI) solutions. The 100ppb and 500ppb dosages were utilized such that reduction and removal could be observed, accounting for the high capacity for removal; it is acknowledged that these values are generally far in excess of natural systems. The machine was purged with at least 250L of water to flush the system and avoid crossover contamination between experiments.

Experiments were run with TiO_2 dosing of 0g/L, 0.01g/L, 0.1g/L and 1.0g/L P90 (TiO_2, >99.5%, Evonik, formerly Degussa). P90 has a higher surface area and photocatalytic activity under UV irradiation than P25 (Doudrick, et. al 2012), and was therefore chosen for this study. Preliminary investigations using the Photo-Cat revealed identical removal efficiencies both with and without an added hole scavenger (e.g., formic acid). Therefore, no organic hole scavengers were used, which would have also decreased pH. Because up to four lamps could be powered simultaneously, experiments using 0, 1, 2, 3, and 4 lamps were completed to assess impact of illumination quantity in hexavalent and total chromium removal. Methylene blue dye tests were used to assess performance degradation over time as well as ongoing quality assurance; all methylene blue tests were allowed 15 min dark adsorption before initiating lamp warm up. Methylene blue dye testing proved comparable performance for all lamps individually as well as similar trends for runs with 1, 2, 3, and 4 lamps. It was found that there is a 9 minute 'delay' for the lamps to fully warm up and begin removal, after which time reduction of methylene blue occurred. This time was factored into experimental design and data energy analysis.

Temperature was regulated to 27.5^{o}C +/- 2.5^{o}C by running cooling water across the lamps. pH was controlled between 8.5 and 8.7 for experiments using deionized water by addition of 5mM $NaHCO_3$, whereas pH for ultrapure (without a buffer) experiments ranged from 6.5 to 7.1. Dechlorinated tap experiments were unbuffered and pH values ranged between 7.7 and 7.9. City of Tempe tap water is hard (220mg/L as $CaCO_3$) (City of Tempe, 2012), and contains primarily carbonate alkalinity. Temperature and pH readings were taken using a Beckman-Coulter pH meter, calibrated before each

experiment. Conductivity readings were taken using a VWR conductivity meter; average conductivity for tap water was 0.9-1.1 mS/cm.

Data Processing

All experiments run were conducted using equivalent energy sampling times to normalize data across experiments. A manufacturer spreadsheet was provided to determine the energy output based on the volume of water being recirculated, number of lamps utilized and the amount of time the lamps were running. Manual calculations of energy were conducted to ensure that the spreadsheet was providing accurate energy inputs. The fundamental equation utilized in this calculation is as follows:

$$Power\ Required = \frac{0.22kW \times N \times t \times 1000}{60 \times V},$$

where 0.22kW represents the amount of power output from each 220W lamp in kW, N represents the number of lamps operational from zero to four, t represents the time the sample was taken in minutes, and V is the recirculation volume utilized in liters. These 'power required' values are the 'energy' portrayed on the x-axes in graphical displays of data.

Upon completion of experiments, an electrical energy per order removal (EE/O) calculation was undertaken to determine energy efficiency of the system. EE/O is defined as the number of kilowatt hours of electrical energy required to reduce the concentration of a pollutant by 1 order of magnitude (90%) in a unit volume of contaminated water (Behnajady, et. al 2009; Behnajady, et. al, 2011; Daneshvar, et. al, 2005). This is represented mathematically:

$$E_{EO} = \frac{P_{el} \times t \times 1000}{V \times 60 \times \log(\frac{[C_0]}{[C]})},$$

where P_{el} is the input power in kWh of the lamps, t is the irradiation time in minutes, V is the volume of water in the reactor in liters, and C_o and C represent the contaminant concentration at time t=0 (initial) and final time under investigation, respectively. For this investigation, this equation can be simplified due to the preliminary calculations for power required (in kWh/m^3) which then simplifies the EE/O calculation to:

$$E_{EO} = \frac{Power\ Required}{\log(\frac{[C_o]}{[C]})}.$$

An EE/O value of less than 0.265kWh/m^3 is both cost and energy 'efficient' and could be reasonably scaled to full scale treatment (Crittenden 2012, 1468).

Chemicals and Materials

Water samples were prepared by spiking 500μg/L hexavalent chromium to either 1) buffered deionized water with 5mM sodium bicarbonate ($NaHCO_3$, Polystormor AR (ACS), >99.7%), 2) 18MΩ deionized nanopure water or 3) dechlorinated tap water (220ppm hardness, 615ppm total dissolved solids on average in Tempe tap water; Tempe, 2012). Potassium dichromate ($K_2Cr_2O_7$, >99%, Sigma Aldrich) was used as the source of the hexavalent chromium. Chromium (III) chloride hexahydrate ($CrCl_3 \cdot H_2O$, >98%, Sigma-Aldrich) was used as the source of trivalent chromium. P90 (TiO_2, >99.5%, Evonik, formerly Degussa) was used as the commercial TiO_2 photocatalyst and was obtained in powder form. P90 contains both anatase (88%, 12nm) and rutile (12%, 18nm) crystal structures, has a surface area of 104m^2/g, and has an average isoelectic point (IEP) of 6.4 (Doudrick, et al. 2012; Doudrick, et al 2013).

Analytical Methods

Aqueous Concentrations and Analysis

All aqueous concentrations were determined from 40mL samples taken from the effluent port after the ceramic membrane. These samples were filtered with 0.45μm filter into a smaller sample volume for analysis on IC or ICP-MS as described below. Preparation for the instruments consisted of adding 2-3% nitric acid (ULTREX, Sigma Aldrich) for the ICP-MS or adding 1% of an ammonium hydroxide buffer for the IC.

Hexavalent chromium concentrations were measured using ion chromatography (Dionex ICS 2000) following a manufacturer recommended modification of EPA Method 218.6 (Sensitive Determination of Hexavalent Chromium in Drinking Water, Thermo Scientific). This method utilizes colorimetric 1,5 diphenylcarbazide post-column reageant and ammonium sulfate eluent to specifically determine the concentration of hexavalent chromium.

Total chromium concentrations were measured using a Thermo Fisher Scientific XSeries 2 quadrapole ICP-MS and Cetac ASX-520 autosampler. Sample introduction consisted of a conical spray chamber with impact bead and concentric nebulizer with a flow of 1ml/min. The spray chamber was cooled to 3 °C by a Peltier cooling system. Collision Cell Technology (CCT) mode was utilized to reduce interferences by the argon gas used to generate the plasma by using a mixture of 7% hydrogen/93% helium. The differential between total chromium and hexavalent chromium was determined to be trivalent chromium.

Samples for aqueous titanium analysis were collected from a sample port (Figure 1) on the reactor as the permeate from the ultrafiltration membrane. Single particle ICP-

MS (spICP-MS), an emerging nanoparticle quantification and size characterization technique (Degueldre, et al. 2005; Mitrano, et al. 2012), was used to evaluated the particulate TiO_2 equivalents amount in the effluent of photocatalyst reactor. Effluent samples were introduced into the ICP-MS directly and the instrument signal in counts per second (cps) was documented versus time. Dwell time, i.e. the unit time interval in which one reading was integrated, was set as 10ms and the sample flow rate was set as 0.69 ml/min. Nebulizer transport efficiency was determined based on previous research (Pace, et al. 2011) as 1.58% to be used in Ti quantification. Total Ti concentration was evaluated by taking account of the elevated baseline relative to the blank and counting the pulses that stand for the detectable particle signals.

Slurry Analysis: Characterizing the Surface

TiO_2 from the effluent slurry of the ceramic membrane was dried at 100^{o}C and then prepared for analysis on scanning electron microscopy (SEM), Fourier transform infrared spectroscopy (FTIR), and x-ray photoelectron spectroscopy (XPS). For SEM analysis, about 0.1 g of sample was put on the surface of the stub. Prepared samples were dried in the air at room temperature (22 °C) before electron microscopy work. Scanning electron microscopy equipped with an energy dispersive X-ray microanalysis system (SEM/EDX) (Philips XL30) was used to locate and characterize chromium on the surface of titanium dioxide.

XPS was used to determine surface elemental composition and chemical state of the chromium and titanium dioxide. XPS was performed on a ESCALAB 220i-XL (Vacuum Generators, USA) with a monochromatic Al Kα source at hν = 1486 eV and a base pressure = 7×10^{-10} mbar.

FTIR was run on two different instruments, a Thermo Nicolet 6700 FTIR and Continuum Microscope System available in Arizona State University Biodesign Institute and a Bruker FT-IR/FT-Raman IFS 66V/S from the LeRoy Eyring Center for Solid State Science. Both instruments utilize liquid nitrogen for cooling. The Nicolet FTIR utilizes transmittance measurements from a diamond and directly analyzes powdered samples placed on the stage. The Bruker FT-IR set up uses mid-IR wavelengths to target absorbance of sample constituents in KBr pellets.

CHAPTER 3

RESULTS

Model Water Testing

Cr(VI) was slowly removed by direct photolysis, without TiO_2 (Figure 2). A 1g/L dosage was found to be the most effective in removing hexavalent chromium, achieving removal to non-detect levels in a very short time, and therefore the low energy input. An unexpected finding was that photolysis (no added TiO_2) was more effective at removal than adding a very low dosage of 0.01g/L. It is likely that the low TiO_2 dosages reduced UV transmittance, thus limiting direct photolysis of Cr(VI), while providing minimal surface for electron transfer to Cr(VI). EE/O calculations were performed to provide a normalized assessment of removal on an energy out of the wall basis (Figure 3). The highest titanium dioxide dose (1.0g/L TiO_2) had an EE/O value of 0.36kWh/m^3, which is within the range suggested to be cost effective (Crittenden, 2012). EE/O values for photolysis and 0.01 g/L TiO_2 are extremely high (22 kWh/m^3 and 54kWh/m^3, respectively), with 0.1g/L TiO_2 also in a very high range (8.3kWh/m^3). Based upon these findings, two TiO_2 dosages (0.1g/L and 1.0g/L) were tested for varied water matrix and under different irradiance conditions.

Tandem Hexavalent Chromium Reduction and Total Chromium Removal

For experiments using dechlorinated tap water spiked with different initial Cr(VI) concentrations, both the hexavalent and total chromium concentrations decreased at the same rate, indicating that both hexavalent and total chromium were simultaneously removed from the aqueous solution (Figure 4). For inputs of 1g/L TiO_2, it was found that removals varied between 89% and 98% for initial concentrations of 500ppb Cr(VI). Only

4% dark adsorption of Cr(VI) onto TiO_2 was found for recirculation under zero irradiance for 1 hour. Thus, all removals above 4% are attributed to photocatalytic processes. With only 0.1g/L TiO_2 added and 100ppb Cr(VI), removals varied from 45% to 70% with around 6.5% dark adsorption.

After Cr(VI) concentrations in the ceramic membrane permeate water decreased to below detection levels, continued and prolonged UV irradiation indicate "reformation" of Cr(VI). This likely occurred as a surface-bound Cr(III) was oxidized to Cr(VI). Reformation potential was tested using an initial input of trivalent chromium instead of hexavalent chromium. Experiments were conducted with 0.1g/L P90 at 100ppb initially available Cr(III) and 1.0g/L P90 at 500ppb initially available Cr(III). Figure 5 shows that in both cases, Cr(VI) evolved from the Cr(III) initial solution, though at a significantly lower rate and extent than that of hexavalent chromium reduction in other tests. This may be due to both the high sorption of Cr(III) to TiO_2 and precipitation of $Cr(OH)_{3(s)}$ at neutral pH.

Characterization and Bonding of Titanium Dioxide and Removed Chromium

Analyses conducted on slurry effluent samples taken after experiments showed accumulation of Cr on the surface. While virgin P90 is a pure white, the dried titanium samples from experiments were visually mint green, an indicator of chromium species on the surface of the titanium dioxide.

SEM was conducted on both virgin P90 and a Photo-Cat® slurry effluent from a dechlorinated tap water experiment of 1g/L P90 and 500ppb Cr(VI) to determine presence and quantity of chromium on the surface of titanium dioxide after photocatalysis. SEM analysis results are shown in Figure 6. For the case of virgin P90,

SEM showed only Ti and O present at the surface, with a carbon response from the stub on which the P90 was mounted. The surface of the effluent titanium from the Photo-Cat® was found to have chromium in addition to a number of common tap water constituents (Na, Mg, S, Cl, K, Ca). Though chromium represents a relatively low atomic weight percentage of surface coverage, detection shows that it is present and attached to the surface in some manner.

XPS results from virgin and photocatalytic effluent TiO_2 indicate the presence of chromium on the surface of the TiO_2. Due to charging of the chromium, the exact bonding state and energy state were indeterminable. FTIR conducted on virgin and photocatalytic effluent TiO_2 revealed differences in absorbance response at 1383.4 and 1508.0cm^{-1}.

Water Matrix and Removal Impact

Water matrix experiments were performed using 18.3MΩ/cm^3 nanopure water (Figure 2), buffered deionized water (5mM $NaHCO_{3,}$) and dechlorinated tap water. Varying the dose of P90 in the reactor slurry under constant illumination conditions revealed the presence a threshold of titanium needed in order to see significant reduction (Figure 7). For doses less than 1g/L, it was found that the reduction potential was diminished greatly due to a combination of the following: insufficient reaction sites or electron evolution, matrix interferences, or irradiation shielding of the lamps. At 1.0 g/L TiO_2 and only one lamp providing illumination, a more typical removal curve is achieved. Nanopure water was found to have complete removal at 1g/L dosing as previously discussed. Dechlorinated tap water consistently performed better than 5mM $NaHCO_3$ buffered deionized water, with removal differentials ranging up to 62% for the

highest TiO_2 dose as shown in Figure 7. Adding 5mM $NaHCO_3$ increases pH almost one unit, which creates less thermodynamically favorable conditions for Cr(VI) reduction. Additionally, calcium is more likely to complex with titanium dioxide and form aggregates, which decreases removal capacity.

Energy Dosage and Removal Impact

Figure 8 shows hexavalent chromium removal in dechlorinated tap water with respect to time and energy input. Portraying the 1.0g/L TiO_2 data in terms of time reveals typical removal plots, decreasing quickly at first and tapering off as concentrations reach low levels (~20% remaining). The time plot also shows 90% removal occurring within the first 30 minutes for all varieties of lamps. Looking only at this data, it would be assumed that all lamps combinations greater than zero (1, 2, 3, or 4) perform almost equally over time.

Plotting this same data with respect to energy input reveals different efficiencies of removal due to lamp warm up and energy cost. All concentrations reach a 1-log removal between 16kWh/m^3 and 21kWh/m^3. There is an inverted pattern of hexavalent chromium removal over energy input, with efficiency decreasing as follows: 1 lamp >2 lamps > 3 lamps > 4 lamps >0 lamps. This is most likely due to the energy accounting issue with the 9 minute delay, in which four times the amount of energy is used for the four lamp scenario in comparison to the one lamp scenario. Equivalence occurs when all removals approach the same value at the same energy, at approximately 21kWh/m^3 and 90% removal.

Titanium Dioxide Presence in Membrane Permeate

Figure 9 shows the concentration of TiO_2 in the ceramic membrane permeate for 0.1g/L TiO_2 in 5mM $NaHCO_3$ deionized water as well as in dechlorinated tap water; all samples were taken at a run-time of 15 minutes and analyzed by SP-ICP-MS. The permeate concentrations show a trend based on water matrix, with TiO_2 concentrations from dechlorinated tap water higher for the samples taken with three and four lamps operating but lower for the two lamps and zero lamps operating conditions. In 5mM $NaHCO_3$ buffered deionized water, increased illumination may result in a higher incidence of ionic complexing with titanium, increasing the size of the particles and preventing breakthrough. Overall, the concentrations in the effluent were significantly higher in runs using zero or two lamps than those found in three or four lamp runs. Up to 100μg/L TiO_2 was found in the permeate (zero lamps, buffered deionized water), having passed through the ultrafiltration membrane. Average particle size of dispersed P90 ranges from 12-18nm, whereas ultrafiltration membranes range from 0.1 to 0.001μm, or 1 to 100nm. Reasons for observed variations may be TiO_2 aggregation patterns upon illumination, pH and ionic strength differences (Tong, et. al, 2013; Domingos, et. al 2009) or decreased ability to escape the ultrafiltration membrane upon higher chromium surface loading onto TiO_2 and thus, increased size of TiO_2 particles.

Efficacy as a Flow-Through System

A 625L flow through experiment was completed to assess TiO_2 saturation potential and continuous loading removal capacity for both 10ppb and 100ppb Cr(VI) solutions (Figure 10). The influent concentration was initially decreased, but this removal

steadily declined over the first hour to reach an ongoing pseudo-steady state at ~12% removal, maintained for the duration of the tests. Though TiO_2 appears to reach a saturation point (~125L treated), hexavalent and total chromium were still reduced thereafter. The mechanisms involved in this process include a cycling between Cr(VI) and Cr(III) at saturation, necessitating a TiO_2 recycling and regeneration step to prevent the oxidation and desorption of Cr(III) species on the surface of the TiO_2 (Figure 11).

A threshold of removal capacity is reached when TiO_2 surface sites become saturated. However, this can be overcome, as Purifics designed a TiO_2 recirculation and regeneration pathway that allows all TiO_2 to be reused well beyond a single saturation through desorption via a strong acid (Purifics, 2012). At full scale, one log removal is achievable with a reported EE/O of 1.8 for an influent concentration of 440ppb Cr(VI) (Purifics, personal correspondence 2013). Therefore, it is possible to have a photocatalyst-driven reaction activated by UV lamps that has zero by-products and demands no additional chemicals without immense catalyst demand.

CHAPTER 4

CONCLUSION

The removal capacity of hexavalent chromium was investigated under varied water matrix, titanium dioxide dosage, and energy input using an engineering-scale photocatalytic reactor system. The integrated UV-TiO_2-ceramic membrane system successfully reduces Cr(VI) and removes all aqueous chromium species. Catalyst dosage was the most impactful quality investigated, with the most successful dosage of 1g/L. Water matrix was found have an effect on removal, but UV-TiO_2 photocatalysis can overcome ion interaction and competition with sufficient catalyst and increased energy input. Energy input reaches a threshold of necessity, above which further illumination may cause oxidation of Cr(III) surface species to aqueous Cr(VI). Surface analysis confirmed chromium species are on the surface of the TiO_2 in the effluent slurry. Mechanisms for Cr(VI) reduction and Cr(III) removal were outlined and determined as hexavalent chromium was reduced to trivalent chromium onto titanium dioxide photocatalytically with a conceptual model (Figure 11).

An application of this method would be for utilities or industry that discharge water and need to meet hexavalent chromium permitting standards. A UV-photocatalytic reactor like the one investigated could allow seasonal and on-demand intervention to reduce discharge levels instead of instituting a year-round additional step in the water treatment process for satisfactory removal and reduction. With increasing interest and technology investment in UV applications for water treatment, this intervention method could become more prevalent on a large scale.

REFERENCES

Adler, R.B., A.C. Smith, and R.L. Longini. 1964. *Introduction to Semiconductor Physics.* New York: John Wiley & Sons.

Bahnemann, Detleft W., Ralf Dillert, and K.J. Robertson. 2003. "Photocatalysis: Initial Reaction Steps." In *Chemical Physics of Nanostructured Semiconductors*, by Alexander I. Kokorin and Detlef W. Bahnemann, 183-202. Boston: VSP.

Barrera-Díaz, C. E., Lugo-Lugo, V., & Bilyeu, B. (2012). A review of chemical, electrochemical and biological methods for aqueous Cr(VI) reduction. *Journal of hazardous materials*, *223-224*, 1–12. doi:10.1016/j.jhazmat.2012.04.054

Beaumont, J. J., Sedman, R. M., Reynolds, S. D., Sherman, C. D., Li, L.-H., Howd, R. A., Alexeeff, G. V. (2008). Cancer mortality in a Chinese population exposed to hexavalent chromium in drinking water. *Epidemiology (Cambridge, Mass.)*, *19*(1), 12–23. doi:10.1097/EDE.0b013e31815cea4c

Behnajady, M. A., Vahid, B., Modirshahla, N., & Shokri, M. (2009). Evaluation of Electrical Energy Per Order (EEO) With Kinetic Modeling On The Removal Of Malachite Green By US/UV/H2O2 Process.*Desalination*, *249*(1), 99-103.

Behnajady, M., Eskandarloo, H., Modirshahla, N., & Shokri, M. (2011). Influence of the Chemical Structure of Organic Pollutants on Photocatalytic Activity of TiO2 Nanoparticles: Kinetic analysis and Evaluation of Electrical Energy per Order (EEO). *Digest Journal of Nanomaterials and Biostructures*, *6*(4), 1887-1895.

Benotti, M. J., Stanford, B. D., Wert, E. C., & Snyder, S. a. (2009). Evaluation of a photocatalytic reactor membrane pilot system for the removal of pharmaceuticals and endocrine disrupting compounds from water. *Water research*, *43*(6), 1513–22. doi:10.1016/j.watres.2008.12.04.

Berz, F. 1975. "The Surface Space Charge Layer." In *Surface Physics of Phosphors and Semiconductors*, by C.G. Scott and C.E. Reed, 143-220. London: Academic Press.

Blesa, M.A., A.D. Weisz, P.J. Morando, J.A. Salfity, G.E. Magaz, and A.E. Regazzoni. 2000. "The Interaction of Metal Oxide Surfaces with Complexing Agents Dissolved in Water." *Coordination Chemistry Reviews* 31-63.

Bowden, J.W., M.D.A. Bolland, A.M. Posner, and J.P. Quirk. 1973. "Generalized Model for Anion and Cation Adsorption at Oxide Surfaces." *Nature* 81-83.

Brito, F, J Ascanio, S Mateo, C Hernfindez, and L A. 1997. “Equilibria of Chromate (VI) Species in Acid Medium and Ab Initio Studies of These Species.” *Polyhedron* 16 (21): 3835–3846.

California Environmental Protection Agency, 2011. "Public Health Goal for Hexavalent Chromium (Cr VI) in Drinking Water".

"Case History: Photo-Cat Hexavalent Chromium (Cr6) Removal to <1ppb."*Purifics*. N.p. n.d. Web. 21 Feb.2013.<www.purifics.com/downloads/Case%20History%20Hexavalent %20Chromium%20Removal.pdf>.

Chakrabarti, S., Chaudhuri, B., Bhattacharjee, S., Ray, A.K., Dutta, B.K., 2009. "Photo-Reduction of Hexavalent Chromium in Aqueous Solution in the Presence of Zinc Oxide as a Semiconductor Catalyst", Chem. Eng. J. 153:86-93.

Chen, D., & K. Ray, A. (2001). Removal of toxic metal ions from wastewater by semiconductor photocatalysis. *Chemical Engineering Science*, *56*(4), 1561–1570. doi:10.1016/S0009-2509(00)00383-3.

Crittenden, John C.. *MWH's water treatment principles and design.*. 3rd ed. Hoboken, N.J.: John Wiley and Sons, 2012. Print.

Costa, M. (1997). Toxicity And Carcinogenicity Of Cr(VI) In Animal Models And Humans. *Critical Reviews in Toxicology*, *27*(5), 431-442.

Cunningham, J. 1988. "Photoeffects on Metal Oxide Powders." In *Surface and Near Surface Chemistry of Oxide Materials*, by Janusz Nowotny, Dufour and Louis-Claude, 345-412. Amsterdam: Elsevier.

Cunningham, J., E.L. Goold, and J.L.G. Fierro. 1982. "Reactions Involving Electron Transfer at Semiconductor Surfaces. Part 11.—Oxygen Isotope Exchange via Photoinitiated R1, R0 and Place Exchange Processes on ZnO and TiO2." *Journal of the Chemical Society: Faraday Transactions I* 785-801.

Dayan, a D., & Paine, a J. (2001). Mechanisms of chromium toxicity, carcinogenicity and allergenicity: review of the literature from 1985 to 2000. *Human & experimental toxicology*, *20*(9), 439–51. Retrieved from http://www.ncbi.nlm.nih.gov/pubmed/11776406.

Daneshvar, N., Aleboyeh, A., & Khataee, A. (2005). The Evaluation of Electrical Energy per Order (EEO) for Photooxidative Decolorization of Four Textile Dye Solutions by the Kinetic Model. *Chemosphere*, *59*, 761-767.

Degueldre, C., Favarger, P.Y., Wold, S., 2006. "Gold Colloid Analysis by Inductively Coupled Plasma-Mass Spectrometry in a Single Particle Mode", *Anal. Chim. Acta*. 555(2):263-268.

Domingos, R.F., Tufenkji, N., Wilkinson, K.J., 2009. Aggregation of titanium dioxide nanoparticles: role of a fulvic acid. *Environmental Science & Technology* 43 (5), 1282e1286.

Doudrick, K., Monzón, O., Mangonon, A., Hristovski, K., Westerhoff, P., 2012. "Nitrate Reduction in Water Using Commercial Titanium Dioxide Photocatalysts (P25, P90, and Hombikat UV100)", J. Environ. Eng.-ASCE. 138(8):852-861.

Doudrick, K., Yang, T., Hristovski, K., & Westerhoff, P. (2013). Applied Catalysis B : Environmental Photocatalytic nitrate reduction in water : Managing the hole scavenger and reaction by-product selectivity. *"Applied Catalysis B, Environmental", 136-137*, 40–47. doi:10.1016/j.apcatb.2013.01.042.

Duro, L, J Bruno, and B. Honeyman. 2001. "Proposal for the Development of Predictive Surface Complexation Models (SCM) to be Used as a Supporting Tool to Kd Parameters in Ka." In *Radioactive Waste Management: Using Thermodynamic Sorption Models for Guiding Radioelement Distribution Coefficient (Kd) Investigations*, by Nuclear Energy Agency OECD, 120-124. Paris: OECD Publishing.

Elliott, R.J., and A.F. Gibson. 1974. *An Introduction to Solid State Physics and its Applications.* New York: Harper & Row; Barnes & Noble.

Flesch, Peter. 2006. *Light and Light Sources: High-Intensity Discharge Lamps.* Heidelberg: Springer.

Gerrity, D., Ryu, H., Crittenden, J., & Abbaszadegan, M. (2008). Photocatalytic inactivation of viruses using titanium dioxide nanoparticles and low-pressure UV light. *Journal of environmental science and health. Part A, Toxic/hazardous substances & environmental engineering*, *43*(11), 1261–70. doi:10.1080/10934520802177813.

Giller, Henk F.J.I. 2000. "A Review of UV Lamps." *Proceedings of the Water Environment Federation* (Water Environment Federation) 1-7.

Gimenez, J., Aguado, M.A., Cervera-March, S. (1996). Photocatalytic reduction of chromium (VI) with titania powders in a flow system . *Kinetics and catalyst activity, 169*(95).

Goldberg, Sabine. 1995. *Adsorption Models Incorporated into Chemical Equilibrium Models.* Chemical Equilibrium and Reaction Models, Madison: Soil Science Society of America.

Henderson, Michael a. 2011. “A Surface Science Perspective on TiO2 Photocatalysis.” *Surface Science Reports* 66 (6-7) (June): 185–297. doi:10.1016/j.surfrep.2011.01.001. http://linkinghub.elsevier.com/retrieve/pii/S0167572911000100.

Hingston, Frank J. 1981. "A Review of Anion Adsorption." In *Adsorption of Inorganics at Solid-Liquid Interfaces*, by Marc A. Anderson and Alan J. Rubin, 51-90. Ann Arbor: Ann Arbor Science.

Howe, Russell F, and Michael Gratzel. 1985. “EPR Observation of Trapped Electrons in Colloidal TiO2.” *Journal of Physical Chemistry* 89 (7): 4495–4499.

Israelachvili, Jacob N. 2011. *Intermolecular and Surface Forces.* Academic Press.

Jinno, Masafumi, Hisayoshi Korukawa, and Masaharu Aono. 1999. "Fundamental Research on Mercuryless Fluorescent Lamps I - Inner Electrode Operation with Pulsed Discharge." *Jpn. J. Appl. Phys* 4608-4612.

Jinno, Masafumi, Masahiro Okamoto, Masashi Takeda, Motomura, and Hideki. 2007. "Luminance and Efficacy Improvement of Low-Pressure Xenon Pulsed Fluorescent Lamps by Using an Auxiliary External Electrode." *J. Phys. D.: Appl. Phys.* 3889-3895.

Kinniburgh, David G., and Marion, L. Jackson. 1981. "Cation Adsorption by Hydrous Metal Oxides and Clay." In *Adsorption of Inorganics at Liquid Solid Interfaces*, by Marc A. Anderson and Alan J. Rubin, 91-160. Ann Arbor: Ann Arbor Science.

Kolansinski, Kurt W. 2009. *Surface Science: Foundations of Catalysis and Nanoscience.* Chichester: John Wiley & Sons.

Kolle, Ulrich, Jacques Moser, and Michael Gratzel. 1985. "Dynamics of Interfacial Charge-Transfer Reactions in Semiconductor Dispersions. ." *Inorganic Chemistry* 2253-2258.

Ku, Y., & Jung, I. L. (2001). Photocatalytic reduction of Cr(VI) in aqueous solutions by UV irradiation with the presence of titanium dioxide. *Water research*, *35*(1), 135–42. Retrieved from http://www.ncbi.nlm.nih.gov/pubmed/11257867.

Lai, H., & Mcneill, L. S. (2006). Chromium Redox Chemistry in Drinking Water Systems, (August), 842–851.

Li, J., Wang, T., & Du, X. (2012). Preparation of visible light-driven SnS2/TiO2 nanocomposite photocatalyst for the reduction of aqueous Cr(VI). *Separation and Purification Technology*, *101*, 11–17. doi:10.1016/j.seppur.2012.09.014.

Liang, Sun, Joon H. Min, Marshall K. Davis, James F. Green, and Donald S. Remer. 2003. "Use of Pulsed UV Processes to Destroy NDMA." *JAWWA* 121-131.

Loo, Ka Hong, Graham J Moss, Richard C Tozer, Senior Member, David A Stone, Masafumi Jinno, and Robin Devonshire. 2004. "A Dynamic Collisional-Radiative Model of A Low-Pressure Mercury – Argon Discharge Lamp : A Physical Approach to Modeling Fluorescent Lamps for Circuit Simulations" 19 (4): 1117–1129.

McNeill, L. S., McLean, J. E., Parks, J. L., & Edwards, M. (2012). Hexavalent Chromium Review, Part 2: Chemistry, Occurrence, and Treatment. *Journal AWWA, 104*(7), 39-40.

Mitrano, D.M., Barber, A., Bednar, A., Westerhoff, P., Higgins, C.P., Ranville, J.F., 2012. "Silver Nanoparticle Characterization Using Single Particle ICP-MS (SP-ICP-MS) and Asymmetrical Flow Field frow Fractionation ICP-MS (AF4-ICP-MS). 27(7):1131-1142.

Micic, OI, and Yuenian Zhang. 1993. "Trapped Holes on Titania Colloids Studied by Electron Paramagnetic Resonance." *Journal of Physical Chemistry* 97: 7277–7283. http://pubs.acs.org/doi/pdf/10.1021/j100130a026.

Noguera, Claudine. 1996. *Physics and Chemistry at Oxide Surfaces.* Cambridge: Cambridge University Press.

Owlad, M., Aroua, M. K., Daud, W. A. W., & Baroutian, S. (2008). Removal of Hexavalent Chromium-Contaminated Water and Wastewater: A Review. *Water, Air, and Soil Pollution, 200*(1-4), 59–77. doi:10.1007/s11270-008-9893-7.

Pace, H.E., Rogers, N.J., Jarolimek, C., Coleman, V.A., Higgins, C.P., Ranville, J.F., 2011.

Rajh, Tijana, Oleg G. Poluektov, and Marion C. Thurnauer. 2003. "Charge Separation in Titanium Dioxide Nanocrystalline Semiconductors Revealed by Magnetic Resonance." In *Chemical Physics of Nanostructured Semiconductors*, by Alexander I. Kokorin and Detlef W. Bahnemann, 1-34. VSP: Boston.

Scanlon, David O, Charles W Dunnill, John Buckeridge, Stephen a Shevlin, Andrew J Logsdail, Scott M Woodley, C Richard a Catlow, et al. 2013. "Band Alignment of Rutile and Anatase TiO_2." *Nature Materials* 12 (9) (September): 798–801. doi:10.1038/nmat3697. http://www.ncbi.nlm.nih.gov/pubmed/23832124.

Schaefer, Raymond, Michael Grapperhaus, Ian Shaefer, and Karl Linden. 2007. "Pulsed UV Lamp Performance and Comparison with UV Mercury Lamps." *Journal of Environmental Engineering and Science* 310: 303–310. doi:10.1139/S06-068. http://www.nrcresearchpress.com/doi/abs/10.1139/s06-068.

Schiavello, Mario. 1997. *Heterogeneous Photocatalysis.* Chichester: John Wiley & Sons.

Schindler, Paul W. 1981. "Surface Complexes at Oxide-Water Interfaces." In *Adsorption of Inorganics at Solid-Liquid interfaces*, by Mark A. Anderson and Alan J. Rubin, 1-50. Ann Arbor: Ann Arbor Science.

Sedman, R. M., Beaumont, J., McDonald, T. a, Reynolds, S., Krowech, G., & Howd, R. (2006, April). Review of the evidence regarding the carcinogenicity of hexavalent chromium in drinking water. *Journal of environmental science and health. Part C, Environmental carcinogenesis & ecotoxicology reviews*. doi:10.1080/10590500600614337.

Seeger, Karlheinz. 2002. *Semiconductor Physics: An Introduction.* Heidelberg: Springer.

Sharma, S. K., Petrusevski, B., & Amy, G. (2008). Chromium removal from water: a review. *Journal of Water Supply: Research and Technology—AQUA, 57*(8), 541. doi:10.2166/aqua.2008.08.

Stumm, Werner. 1992. *Chemistry of the Solid-Water Interface.* New York: John Wiley & Sons.

Sutton, R., 2010. "Chromium-6 in U.S. Tap Water", Environmental Working Group Report.

Taylor, Christopher D., and Matthew Neurock. 2005. "Theoretical Insights into the Structure and Reactivity of the Aqueous/metal Interface." *Current Opinion in Solid State and Materials Science* 9 (1-2) (February): 49–65. doi:10.1016/j.cossms.2006.03.007. http://linkinghub.elsevier.com/retrieve/pii/S1359028606000234.

City of Tempe, 2012. "Water Quality Report", City of Tempe Public Records.

Tong, T., Binh, C. T. T., Kelly, J. J., Gaillard, J.-F., & Gray, K. a. (2013, May 1). Cytotoxicity of commercial nano-TiO2 to Escherichia coli assessed by high-throughput screening: effects of environmental factors. *Water research*. doi:10.1016/j.watres.2013.02.008.

Uhrlandt, D, R Bussiahn, S Gorchakov, H Lange, D Loffhagen, and D Nötzold. 2005. "Low-Pressure Mercury-Free Plasma Light Sources: Experimental and Theoretical Perspectives." *Journal of Physics D: Applied Physics* 38 (17) (September 7): 3318–3325. doi:10.1088/0022-3727/38/17/S37. http://stacks.iop.org/0022-3727/38/i=17/a=S37?key=crossref.fcd74207fbed491646a097c302d62a54.

Vignesh, K., Priyanka, R., Rajarajan, M., & Suganthi, A. (2013). Photoreduction of Cr(VI) in water using Bi2O3–ZrO2 nanocomposite under visible light irradiation.

Materials Science and Engineering: B, *178*(2), 149–157. doi:10.1016/j.mseb.2012.10.035

Voronov, a. 2008. “New Generation of Low Pressure Mercury Lamps for Producing Ozone.” *Ozone: Science & Engineering* 30 (6) (November 25): 395–397. doi:10.1080/01919510802341012. http://www.tandfonline.com/doi/abs/10.1080/01919510802341012.

Wang, L., Wang, N., Zhu, L., Yu, H., Tang, H., 2008. "Photocatalytic Reduction of Cr(VI) over Different TiO2 Photocatalysts and the Effects of Dissolved Organic Species," J. Hazard Mater. 152:93-99.

Wang, X., Pehkonen, S. O., & Ray, A. K. (2004). Removal of Aqueous Cr(VI) by a Combination of Photocatalytic Reduction and Coprecipitation. *Industrial & Engineering Chemistry Research*, *43*(7), 1665–1672. doi:10.1021/ie030580j.

Wani, Koichi. 1994. “Ladderlike Ionization of the Mercury Atom in Hg-Ar Low-Pressure Discharge and Its Modeling.” *Journal of Applied Physics* 75 (10): 4917. doi:10.1063/1.355780. http://link.aip.org/link/JAPIAU/v75/i10/p4917/s1&Agg=doi.

Westerhoff, P., Moon, H., Minakata, D., & Crittenden, J. (2009). Oxidation of organics in retentates from reverse osmosis wastewater reuse facilities. *Water research*, *43*(16), 3992–8. doi:10.1016/j.watres.2009.04.010.

Yang, J.K., S.M. Lee, M. Farrokhi, O. Giahi, and M. Shirzad Siboni. "Photocatalytic Removal of Cr(VI) with Illuminated TiO2." *Desalination and water treatment* 46 (2012): 375-380. Print.

Figure 1 - Schematic of pilot-scale photocatalytic reactor, Photo-Cat L®, by Purifics.

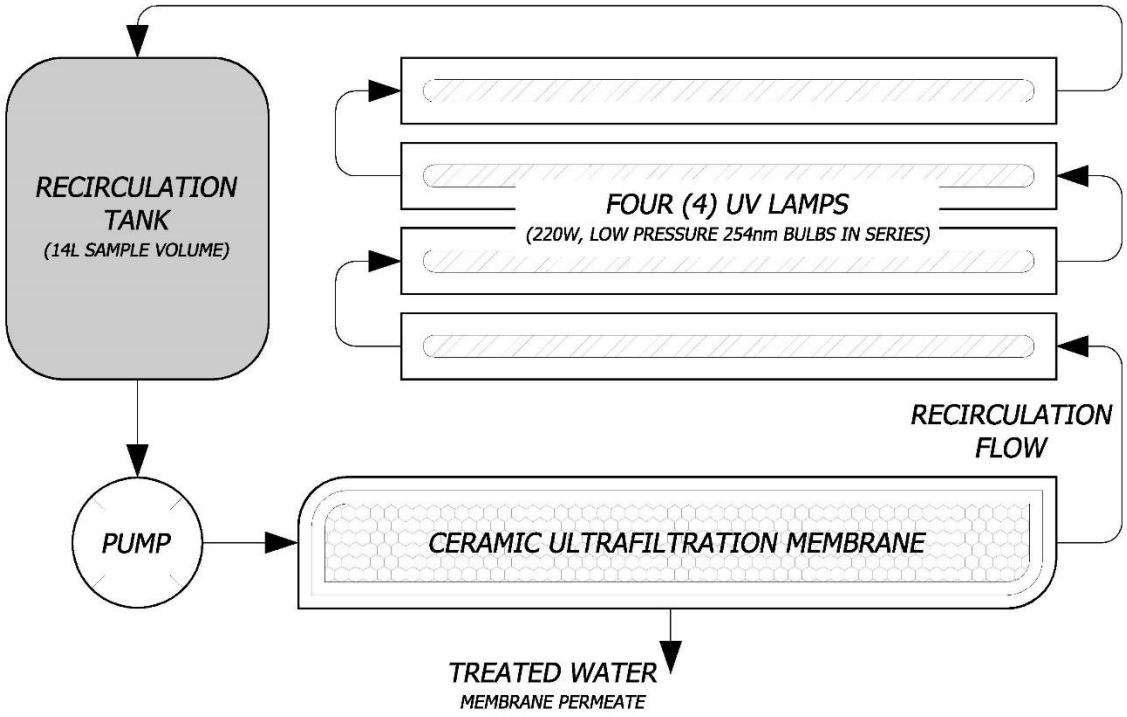

Figure 2 - Hexavalent chromium removal as a function of four P90 TiO_2 catalyst dosages in model water matrix (18.3MΩ nanopure deionized water) with one of four operational lamps running in recirculation mode. pH ranged from 6.5 to 7.1 (initial to final) and temperature was maintained between 25-30ºC.

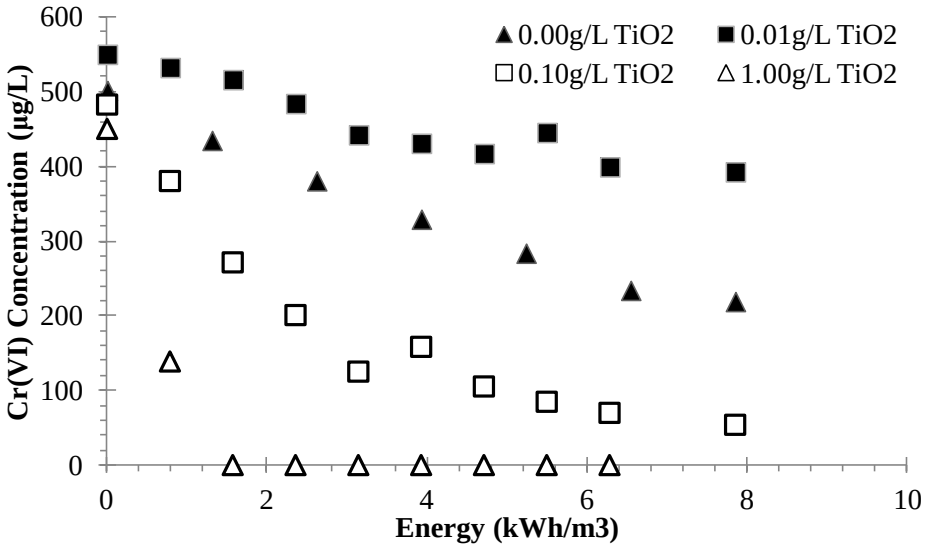

Figure 3 - Electrical energy per order EE/O comparison between varied TiO_2 dosages in a model water (18.3MΩ nanopure deionized water).

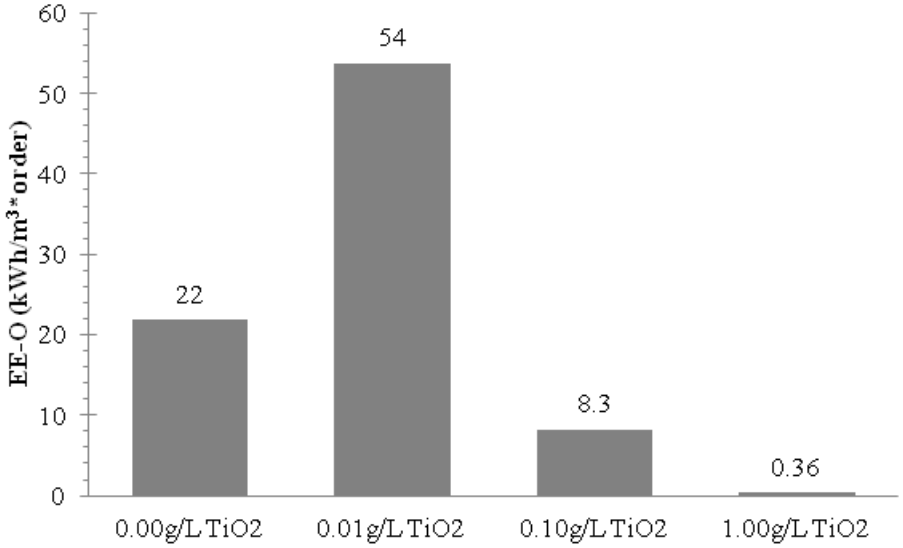

Figure 4 - Removal efficiencies for hexavalent and total chromium in dechlorinated tap water with initial Cr(VI) concentration of 500μg/L. The Y-axis represents calculated removal of either hexavalent or total chromium, while the x axis represents the number of lamps utilized. Zero lamp data represents runtime of one hour of dark adsorption. All other data sets are using removal values normalized to an equivalent energy input (31kWh/m^3).

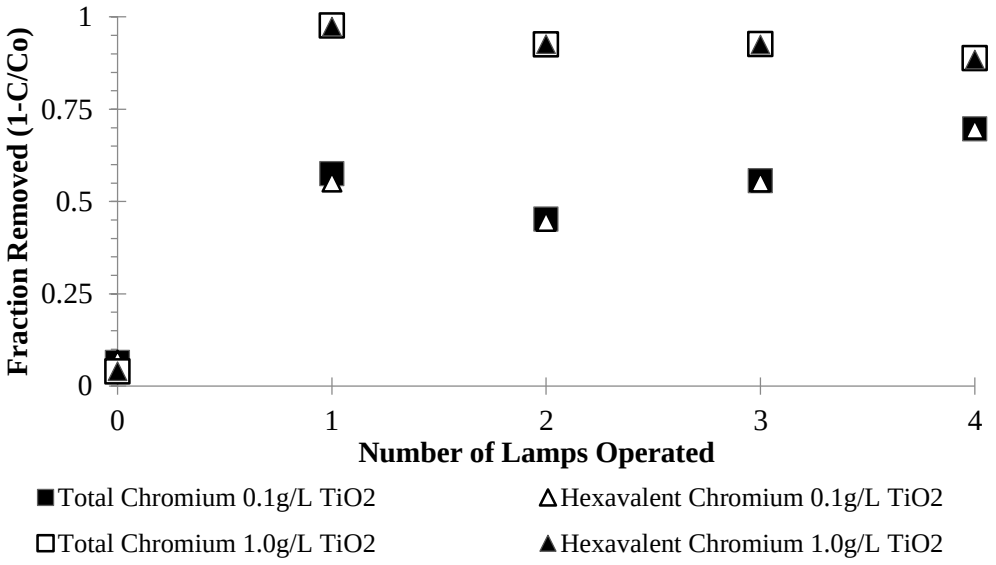

Figure 5 - Evolution of Cr(VI) from starting concentration of only Cr(III) in dechlorinated tap water. pH increased over the course of the experiment (7.5 to 7.75 and 7.85 to 7.95 for 1.0 g/L TiO_2 and 0.1g/L TiO_2, respectively).

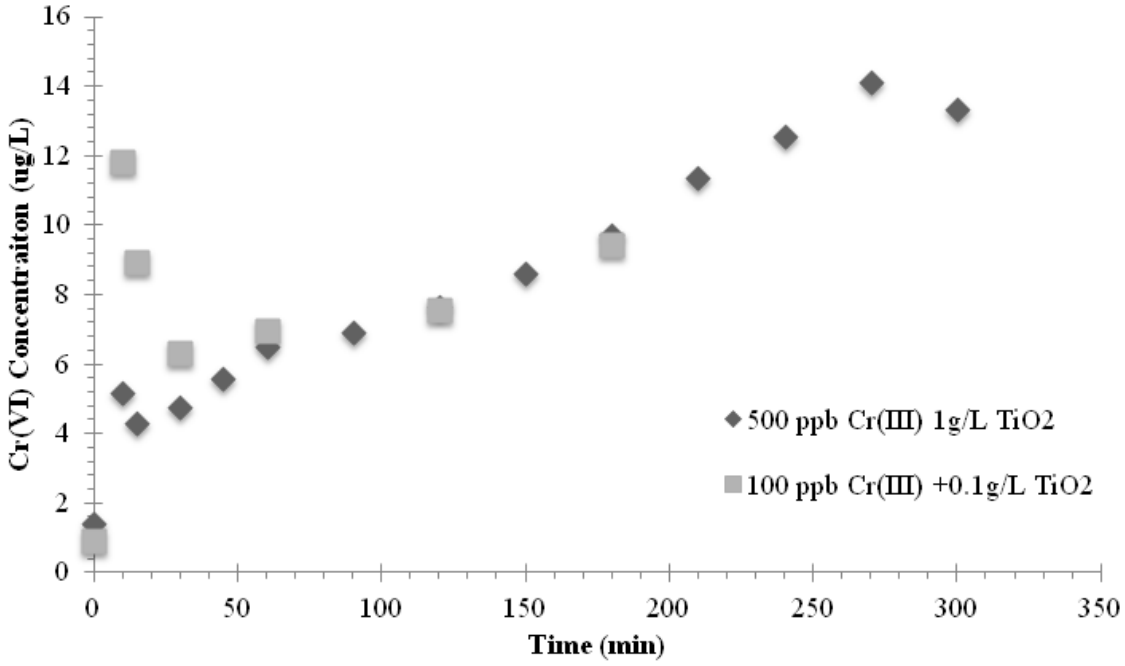

Figure 6 - SEM results indicating the presence of chromium species on the surface of the catalyst.

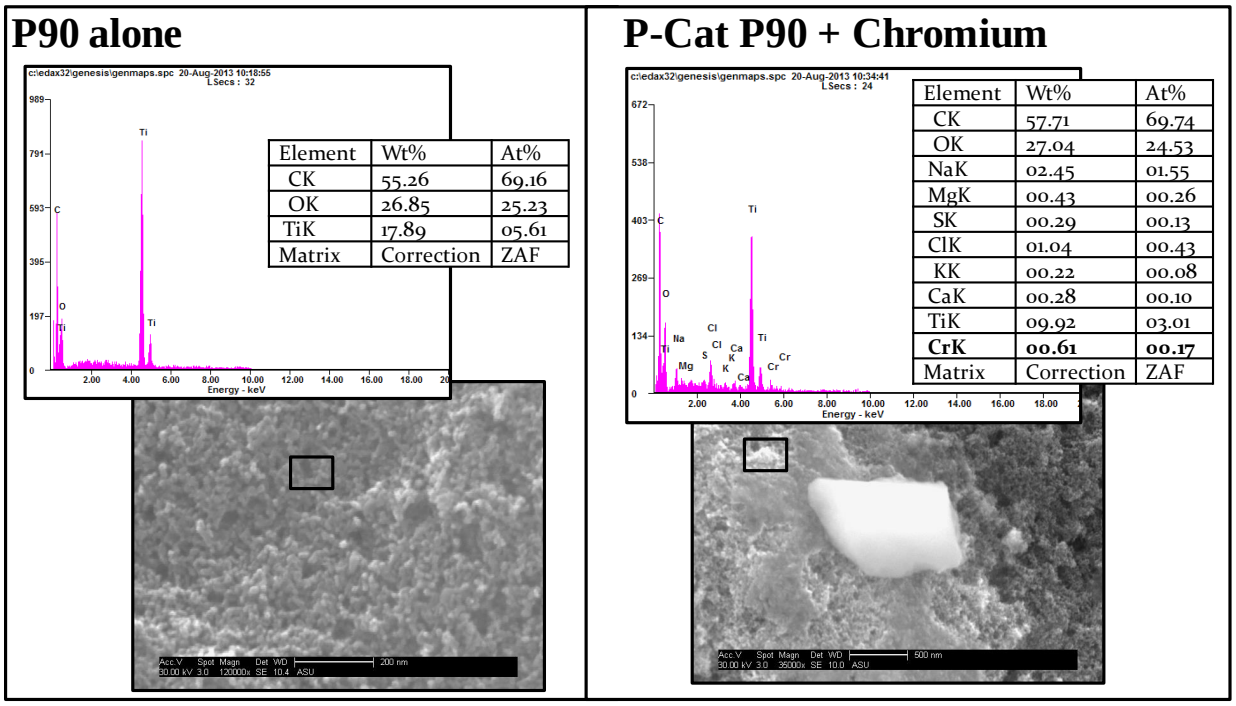

Figure 7 - Effluent chromium concentrations based on initial input P90 dosage. Initial concentrations were 500ug/L Cr(VI) with added 0.0g/L, 0.01g/L, 0.1g/L, 1.0g/L added P90 titanium dioxide. Experiments above were conducted using buffered deionized water (5mM $NaHCO_3$, pH 8.5 to 8.7), unless otherwise noted in the legend. pH for dechlorinated tap matrix ranged from 7.7 to 7.9 from C_{in} (at t=0) to C_f (final sampling); pH for ultrapure ranged from 6.5-7.1. Temperature was controlled to remain between 25ºC and 30ºC for all experiments.

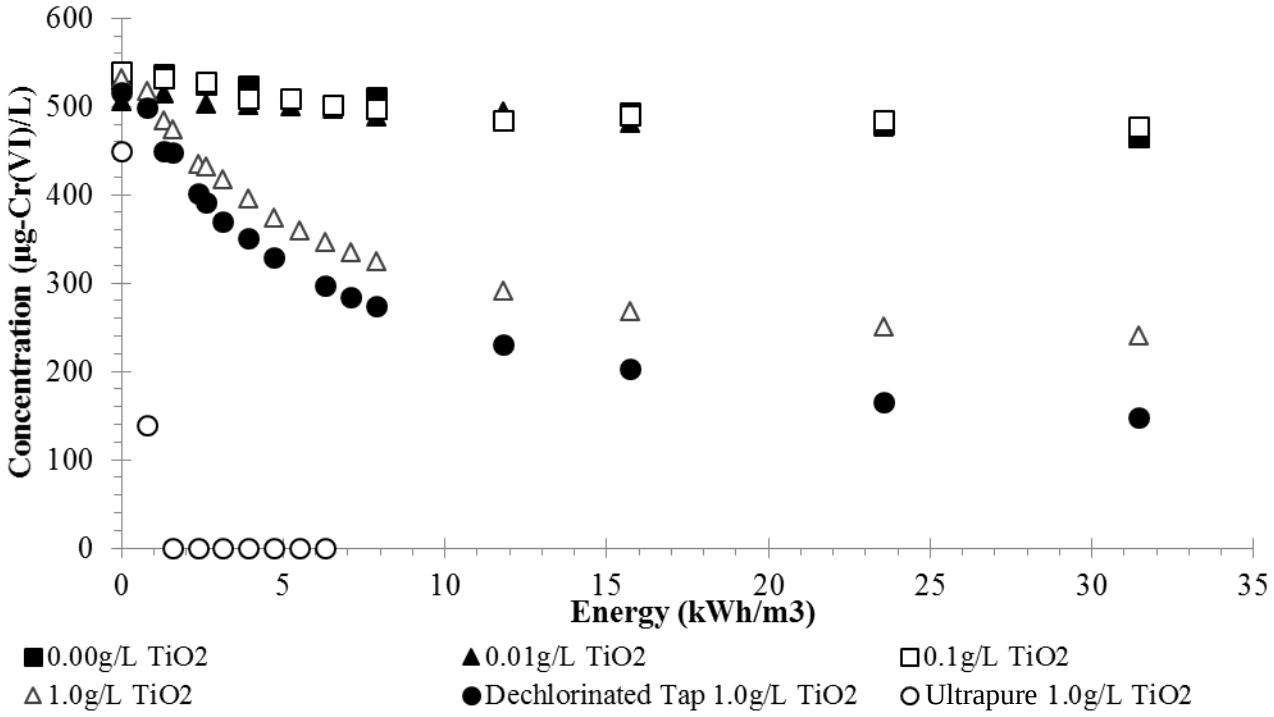

Figure 8 - Comparative assessment of energy dosage for a constant P90 dosage: 1.0g/L P90. Variability across both time and energy input (inset) are shown to show contrasting results between catalyst dosage in dechlorinated tap water matrix.

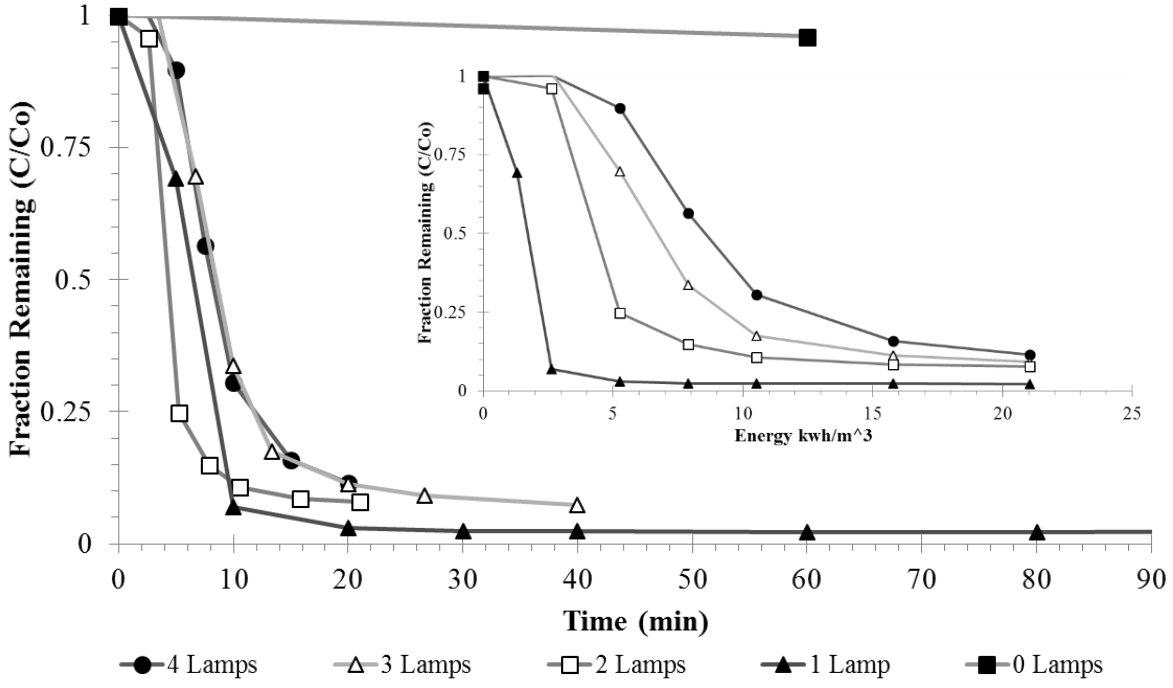

Figure 9 - Titanium dioxide concentration in membrane permeate samples taken at t=15min as a function of lamps and water matrix. pH for 5mM $NaHCO_3$ buffered DI matrix ranged from 8.5 to 8.7 from C_{in} to C_f; pH for dechlorinated tap ranged from 7.7 to 7.9. Temperature was controlled to remain between 25°C and 30°C for all experiments.

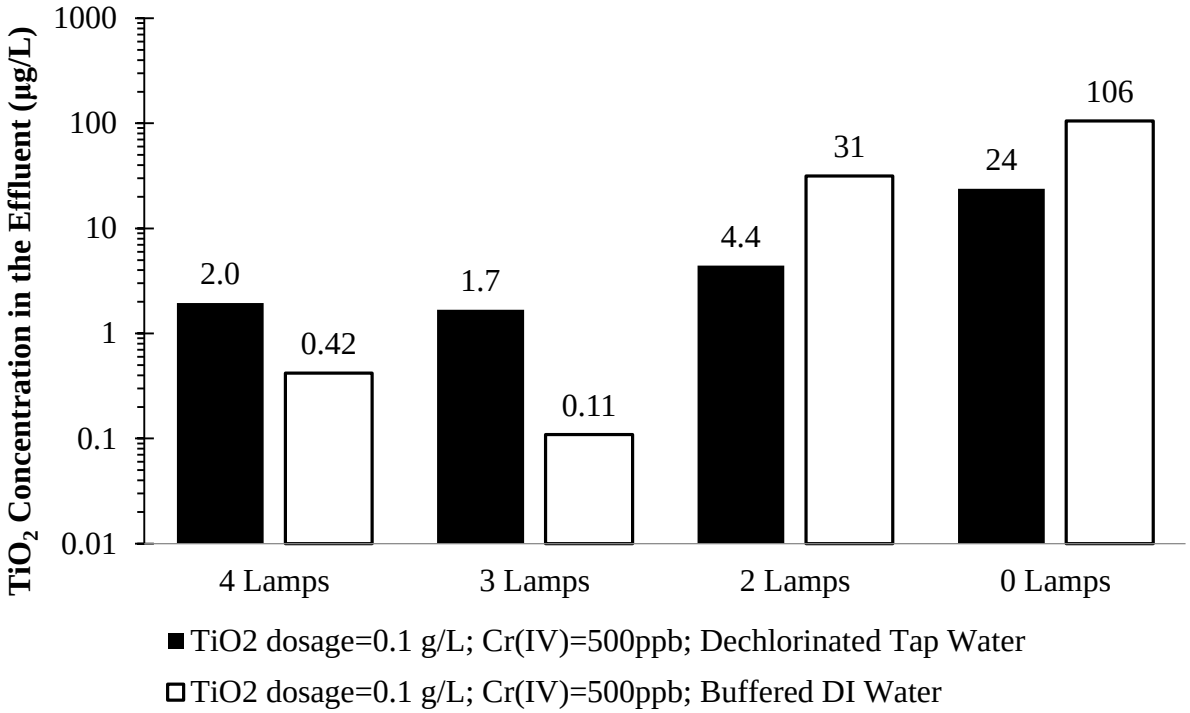

Figure 10 – Hexavalent chromium concentration as a function of time in a flow through (2.1Lpm in/out) mode with a constant 14L internal volume. pH ranged 7.2 (initial) to 7.8 (final) and temperature was maintained at 28ºC +/- 1ºC for both runs (100ppb Cr(VI) and 10ppb Cr(VI) with 1g/L TiO_2).

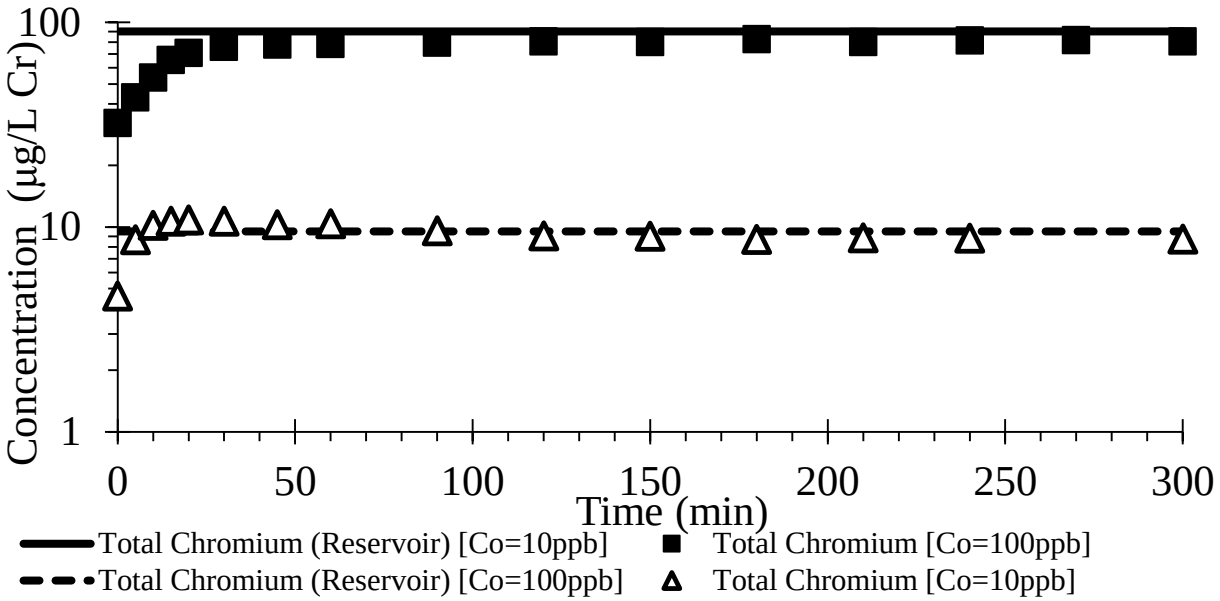

Figure 11 - Conceptualization of mechanisms involved in the reduction of hexavalent chromium and removal from aqueous solution of total chromium species via reduction and sorption processes. Upon significant reaction progression, oxidation and desorption of trivalent species on the surface of titanium yield hexavalent species. The TiO_2 recycle segment advantageously desorbs trivalent chromium after reduction of hexavalent chromium to trivalent chromium using acidic solution. Trivalent chromium is extracted to a 'waste' before it can be oxidized back to aqueous Cr(VI).

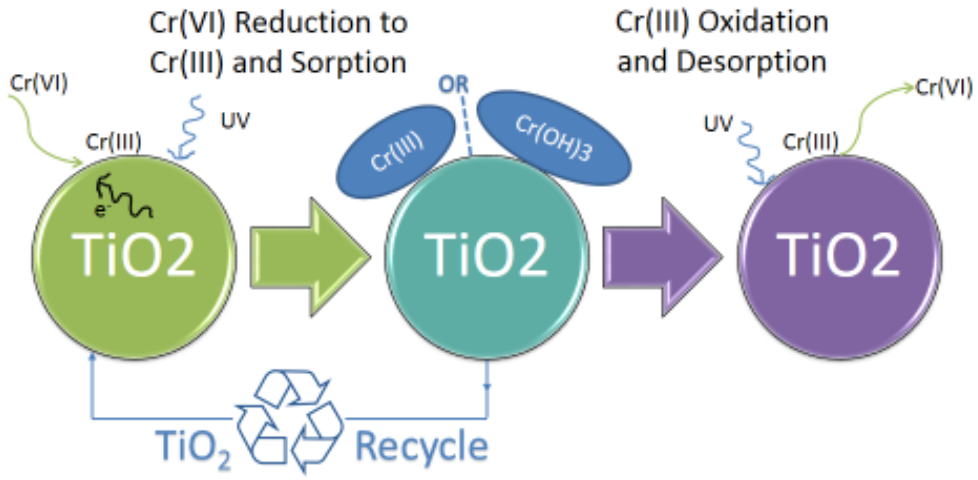

BIOGRAPHICAL SKETCH

Ms. Stancl is a proud undergraduate physics alumnae from Pepperdine University in Malibu, California. She spent three years doing astrophysics research in her undergraduate course of study which prepared her for the research process. As she transitioned to environmental engineering, she was able to pursue her aspirations of providing clean water and helping those around her. Currently in a doctoral program at Arizona State University, she decided to defend a masters in environmental engineering based on her first year of research under Dr. Paul Westerhoff. She is excited to continue learning, researching and growing in her doctoral degree and hopes to become more involved in the engineering applications of her research work.